Spectroscopic measurements on vacuum spark plasmas*

W. A. Cilliers,† R. U. Datla, and Hans R. Griem

University of Maryland, Department of Physics and Astronomy, College Park, Maryland 20742

(Received 19 March 1975)

Photoelectric spectra of the regions corresponding to resonance line emission of He-like ions of titanium, iron, and copper from a low-inductance vacuum spark were obtained, as were spectra of the regions corresponding to $K\alpha$ and $K\beta$ emission from the same elements and to $K\beta$ emission of molybdenum. Electron temperatures are estimated from continuous x-ray emission spectra to $\kappa T_e \lesssim 15$ keV; ion temperatures from x-ray line widths to $\kappa T_i \lesssim 10$ keV. A broad peak superimposed on the visible continuum is interpreted as anomalous bremsstrahlung at twice the electron plasma frequency. The resultant electron density is $N_e \approx 5 \times 10^{20}$ cm^{-3}, consistent with the absence of forbidden He-like ion lines. Experimental observations support the suggestion that the x-ray-producing dense plasmas are due to interactions between pulsed electron beams and low-temperature anode vapors or plasmas.

I. INTRODUCTION

The x-ray spectra of highly stripped ions are receiving considerable attention in a number of laboratories. The main interest in these spectra arises from (1) the desire to identify spectral lines in solar spectra, and (2) the demand for reliable diagnostic techniques in controlled thermonuclear fusion experiments where radiation from high-Z impurities may be important as an energy-loss process. The work presented in this paper deals with spectra from the elements Ti, Fe, Cu, and Mo, generated in a low-inductance vacuum spark described in Sec. II. The electron temperature and density in this device are also important, mainly for interpretation of the results and their application to other plasmas, and two subsections (III C and III D) deal with this. Finally, Sec. IV contains a discussion of a mechanism by which x-ray-producing plasmas may be generated in the vacuum spark, while Sec. V summarizes our conclusions for the dominant operating mode of our apparatus.

II. APPARATUS

Vacuum sparks have been used in one form or another by a number of workers[1-4] for generating x-ray spectra. In spite of various attempts[5,6] at explaining the detailed mechanism responsible for x-ray production in the vacuum spark, some of its characteristics are not fully understood, and improvement in its operation has come about largely through trial and error. Moreover, even a given apparatus may well exhibit more than one operating mode.

Our apparatus originally had a flat cathode and below it a pointed anode separated by about 8 mm and mounted in a vacuum on top of a 30-μF capacitor.[4] (The cathode was later altered as explained below.) Breakdown of the gap was effected by a high-voltage pulse applied to a trigger pin in the cathode. Two Bragg monochromators with flat LiF crystals having a lattice ($2d$) spacing of 2.846 Å were set up 180° to each other. Photomultiplier tubes (1P28) and scintillators (Pilot B) mounted on arms driven at twice the crystal angle by means of goniometers, observed the x rays diffracted by the crystals. Aluminum foil windows protected the crystals from metal vapor emitted from the spark. The base pressure achieved in the common vacuum system used for the spark and monochromators was $\sim 5 \times 10^{-6}$ Torr. Higher base pressures led to reduced x-ray production.

In order to calibrate the monochromators, the following procedure was followed. A mirror (in the exact position of the crystal) was rotated until a laser beam going just above the tip of the anode was reflected into a single 0.5-mm slit in front of the photomultiplier. A Soller slit (0.075°), placed between the anode and mirror and aligned to let the laser beam through, was then "illuminated" with a Cu-targeted x-ray tube, and the $K\alpha$ and $K\beta$ lines were scanned after the crystal was put in place of the mirror. The λ-vs-θ calibration of both monochromators and the $2d$ spacing of the crystals could thus be obtained. Comparison with the manufacturer's values gave a measure of the quality of the calibration. Since the x-ray-producing region in the vacuum spark is very small and serves as a point source, the Soller slit was used only for the calibration. (The theoretical resolution, ~ 0.8 mÅ with the single slit, was almost four times better than that obtainable with the narrowest Soller slit available, $\sim 0.075°$.) With this arrangement, it becomes very important for the x-ray source not to change position in a direction perpendicular to the line connecting the two monochromators. In order to restrict lateral motion of the current path as much as possible, a copper "collar" surrounding the anode and forming part of the cathode was introduced as indicated in Fig. 1. The idea was that image currents in the collar would tend to center the discharge current. With a flat cathode, a crater appears in the anode after some 50 shots. With the collar, a very small but deep hole approximately 1 mm in diameter appears, showing that some stabilization did occur. Further confidence in the wavelength calibration is provided by observing K lines from the anode (see Sec. III B).

The 1P28 photomultiplier tubes had a transit time quoted by the manufacturer as 18 nsec (depending on the voltage), while the spread in transit time was about 2 nsec. The Pilot B scintillators used in front of the photomultipliers had a time resolution also close to 2 nsec.

The discharge circuit had the following parameters: capacitance, 30 μF; total inductance, 23.6 nH; quarter period, 1.3 μsec. The charging voltage was usually 10 kV, and the stored energy was thus 1.5 kJ.

III. MEASUREMENTS AND ANALYSIS

The x-ray flux produced by the vacuum spark as seen by the Bragg monochromators is not reproducible from one shot to the next. In order to overcome this difficulty, the second monochromator was placed on the spectral line to be scanned, and the signal used to normalize that from the scanning monochromator. This procedure was followed on all the scans.

Preliminary scans using copper electrodes showed that both the line x-ray signals and the wavelength resolution of the monochromators were improved by the cathode collar and the single- (rather than Soller-) slit arrangement. The x rays seemed to be characteristic of the anode material rather than the cathode material, and in order to improve the lifetime of the cathode, an insert of Elkonite 3W3 (a copper-tungsten alloy), as shown in Fig. 1, was used.

A. Statistics

When a line was scanned, up to ten shots were taken at each wavelength position. For every shot, a ratio of the peak amplitudes of the two monochromator signals was obtained. Ideally, the ratios should be the same for all shots at a given wavelength position, and if this is approximately true, the same final result will be obtained if one takes the average of the individual ratios or the ratio of the sum of the signals from the monitor and scanning monochromators. Actually, the amplitudes of the signals could vary over an order of magnitude from one shot to the next, and it was found that ratios for the small-amplitude shots tended to increase the standard deviation of the ratios. However, if the correlation between the monitor and scanner signals is good, one is justified in taking the ratio of the average signals instead of the average of the individual ratios. Such a procedure simply means that one integrates the intensities of the two re-

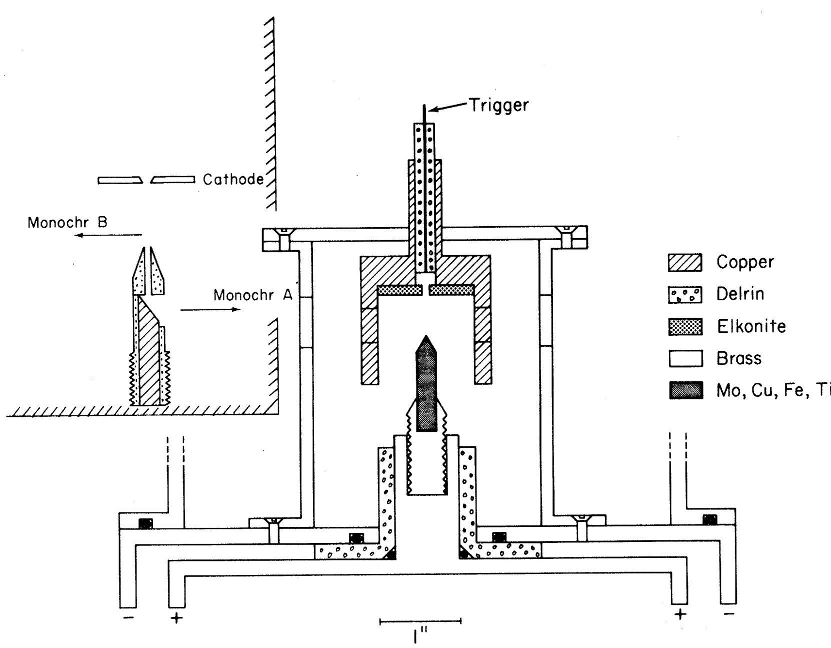

FIG. 1. Vacuum-spark apparatus with cylindrical collar. Modified iron anode used in establishing the presence of intense electron beams is shown in the insert on upper left.

spective signals over a number of shots, thus reducing statistical errors.

For a monitor to be meaningful in the first place, there must exist good correlation between the monitor and scanner signals. To determine this correlation quantitatively, the correlation coefficient for these two signals was calculated for each (scanner) wavelength position for all the spectral scans. The correlation coefficient between two signals x and y is defined by

$$\rho_{xy}=\left(\sum_{i=1}^{N} x_i\, y_i - N\bar{x}\bar{y}\right)\Big/ (N-1)\sigma_x \sigma_y \ ,$$

where N is the number of points and σ_x, σ_y are the standard deviations. A value of $|\rho|=1$ indicates perfect correlation (or anticorrelation), while $|\rho|\approx 0.5$ indicates that, although there may not be perfect point-by-point correlation, there are still rather similar trends between the two curves $x=x(i)$, $y=y(i)$. A nearly vanishing value of $|\rho|$ obviously means that the two curves are completely unrelated.

In Table I we give the average correlation coefficient and its standard deviation for each scan. (Each of the values in the table is the average of between 20 and 30 individual values.) With such high correlation coefficients, one is fully justified in taking the ratio of the average scanner and monitor signals for normalization purposes. Also, instead of putting error limits on each of the individual points in the scans, we note the following: repeating the scans showed that the features that we refer to as the He-like resonance lines have uncertainties of $\pm$ 10% in both amplitude and width, while the Li-like features were found to be less reproducible from one scan to the next, probably because there are many narrow closely spaced lines. Certain features in this region, like the one near the predicted intercombination ($2\,^3P_1$-$1\,^1S_0$) line, appeared on the scans for all three elements, Cu, Fe, and Ti. The correlation coefficients for this part of the spectrum are

TABLE I. Correlation coefficients for spectral scans with monitor positions (in Å) as indicated in brackets.

He- and Li-like	Cu[1.4770]	0.87 ± 0.10
	Fe[1.8510]	0.90 ± 0.11
	Ti[2.6100]	0.90 ± 0.10
$K\beta$	Mo[0.6327]	0.73 ± 0.09
	Cu[1.3890]	0.84 ± 0.12
	Fe[1.7566]	0.92 ± 0.12
	Ti[2.5125]	0.83 ± 0.13
$K\alpha$	Cu[1.5407]	0.91 ± 0.11
	Fe[1.9361]	0.97 ± 0.02
	Ti[2.7486]	0.91 ± 0.08

still high (≈ 0.85), indicating that the lines observed on a particular scan are statistically significant. However, because of uncertainty in wavelength reproducibility ($\pm$ 0.2 mÅ) and possible slight changes in conditions after electrodes have been changed between scans, these features appear somewhat different from one scan to the next. We have accordingly not attempted to identify any of the Li-like satellite lines. An uncertainty of ~20% has to be put on the relative intensities in this region of the spectra.

To further help the reader in deciding on the reliability of a particular part of a spectrum, we have indicated by $\times$ all the points on the scans for which the correlation coefficient was less than 0.6. (This is an arbitrarily chosen value which is still regarded as indicating quite good correlation.) These points were not included in calculating the average values of ρ in Table I.

B. Spectral scans

The following lines were scanned: $K\alpha, K\beta$, Li-like satellites, and He-like resonance lines of the elements Ti, Fe, and Cu ($Z=21$, 26, and 29). The wavelength regions near the hydrogenlike resonance lines for Ti and Fe were also carefully scanned. In addition to the above elements, we scanned the $K\beta$ and hydrogenlike lines of Mo ($Z=42$). In none of these elements could we find any statistically significant hydrogenlike line radiation above the background (~5% of the He-like resonance line). The possibility of at least some of the discharges giving rise to hydrogenlike lines cannot, however, be ruled out. (Density, temperature, and apparent plasma lifetime would all seem sufficient for hydrogenlike lines, at least up to $Z=29$, to appear. See Sec. IV.)

The charging voltage (10 kV) on the bank was sufficiently high to generate characteristic K radiation from the anode material (except Mo) at the beginning of the discharge. This radiation was found useful to obtain an accurate wavelength calibration of the monochromators (~$\pm$ 0.2 mÅ).

a. $K\alpha$ spectra. Apart from the normal K radiation of the various (once-ionized) elements, the corresponding radiations from multiply ionized atoms were also observed. In the case of $K\alpha$, House[7] has calculated the expected wavelengths. According to his calculations, the radiation, e.g., from Fe X is expected to be at a longer wavelength than that of the normal $K\alpha$, while lines from more highly stripped ions are predicted at shorter wavelengths. Our scans for $K\alpha$ of Cu and Ti are given in Figs. 2(a) and 2(b), respectively. (The Fe spectrum is similar to those presented.) The main characteristic of the observed spectra is

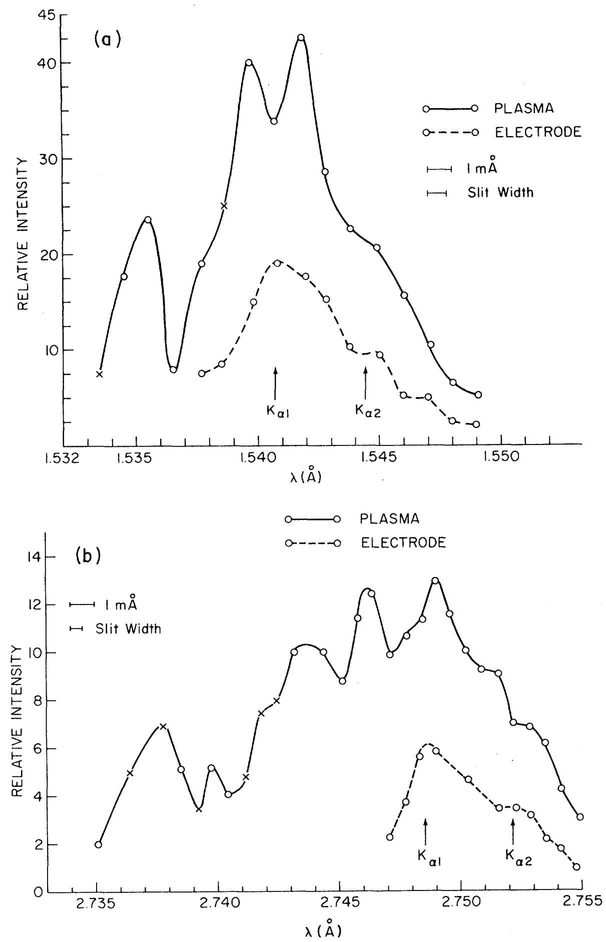

FIG. 2. $K\alpha$ radiation [monitor position in brackets]: (a) Cu [1.5407 Å], (b) Ti [2.7486 Å]. All intensities are estimated to have ±10% accuracy, except for the points marked × (see text). Wavelength errors are ≲0.2 mA.

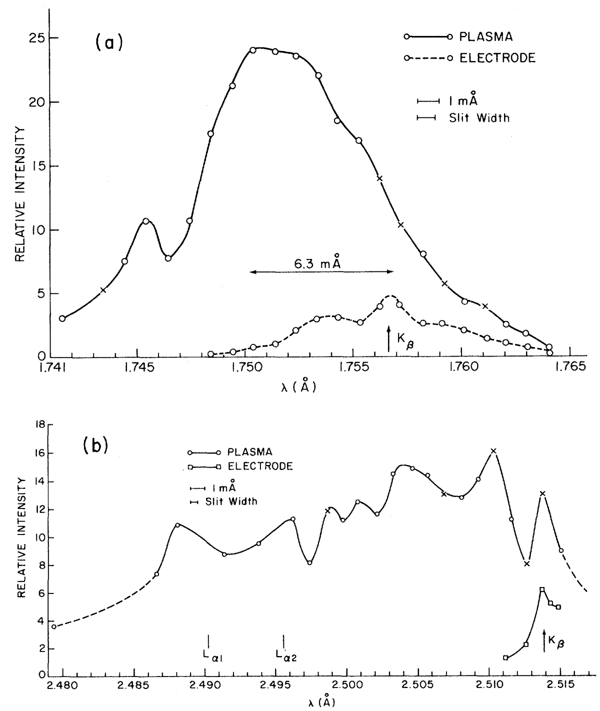

FIG. 3. $K\beta$ radiation [monitor position in brackets]: (a) Fe [1.7566 Å], (b) Ti [2.5125 Å]. Intensity and wavelength errors as in Fig. 2. The horizontal arrows indicate the separation of the observed intensity maximum from the normal $K\beta$ line.

that they are extended towards the short-wavelength side. As a result of this, the $K\alpha_1$ and $K\alpha_2$ lines are no longer clearly separated. The individual lines from different ions are not resolved. No shift towards longer wavelength[4] could be established within the accuracy of our measurements, although this conclusion is preliminary, pending an interpretation of the profile structures.

b. $K\beta$ spectra. In Figs. 3(a) and 3(b) the $K\beta$ spectra of Fe and Ti are given and also the normal $K\beta$ spectra from the anode material. These occur at an earlier time than the main (plasma) spectra, as mentioned above. In the case of Mo (not presented), the intensity peak of the plasma $K\beta$ blend occurs near the expected position of the normal (Mo II) $K\beta$ line. (The 10-kV charging voltage was not high enough to generate this line from the anode material, which requires ~20 keV.) For the other elements (including Cu), the plasma radiation at the normal line position was relatively weak, such that the peak intensity occurs at a wavelength about 6 mÅ below the normal position for Cu and Fe. In these two cases the intensity drops rather sharply towards lower wavelengths beyond the peak, and the shapes of the spectra are practically the same. Estimates using Hartree-Fock energy tables[8] suggest that the intensity peaks correspond to K- or Ar-like ions, Fe VIII–IX, Cu XI–XII, Ti IV–V. Much more accurate calculations by Fraenkel, Klappish, and Schwob[9] for Fe confirm this assignment. In the case of Ti, the hydrogenlike resonance lines lie on the short-wavelength side of $K\beta$ and close to it. If any H-like radiation for this element was present, it would be blended with the shifted plasma $K\beta$ radiation. In Fig. 3(b) the expected positions of $L\alpha_1$ and $L\alpha_2$ are given. It is obvious that no firm conclusion about the absence or presence of these lines can be drawn, except to say that they would have to be rather weak. (In Ref. 2, intensities at these positions were sufficiently strong for positive identification.)

c. He-like resonance and intercombination lines. In the cases of Cu, Fe, and Ti, relatively strong lines were detected at or close to predicted positions of these lines. (In particular, for Fe and Cu we detected intensity maxima within ± 0.4 mÅ from predicted positions[10–12] of the $^3P_1$-$^1S_0$ transitions.) On the long-wavelength side of the He-like resonance line are Li-like satellite lines.[12] Scans covering all these lines are given in Figs. 4(a) and 4(b) for the elements Cu and Fe, respectively. The striking feature of the He-like resonance line is its large half-width of about 5 mÅ (also in the case of Ti). The intercombination ($^3P_1$-$^1S_0$) line, on the other hand, has an apparent half-width of only about 1.7 mÅ. This precludes Doppler broadening as a major cause for the width of the resonance line. A more plausible explanation is that the resonance line is blended with Li-like satellite lines[13,14] originating from ions with the third electron in $n \geq 3$ levels, although the relative strength of Li- and He-like features varies from element to element. (Perhaps Be-like satellites ought to be considered as well.) Summers[13] and Gabriel[14] have done some calculations showing that such satellites could fall on either side and close to the resonance line. At least part of the lines identified as He-like resonance lines may therefore arise from lower ionization stages, and the true total intensities of the He-like resonance lines are most likely much smaller than indicated by our scans. This interpretation is consistent with the rather weak and narrow intercombination line. The forbidden ($^3P_2$-$^1S_0$) line is absent in all three cases.

d. Li-like satellite lines. Gabriel[12] has done calculations of both the wavelengths and intensities relative to the He-like resonance line for the $n = 2$ Li-like satellite lines. The two processes for generation of these lines considered by him are inner-shell excitation and dielectronic recombination. Of these two, inner-shell excitation is probably the dominant process in high-density, transient (rapidly ionizing) laboratory plasmas. Since the satellite lines are not resolved in our case, and since the contribution of $n \geq 3$ satellite lines is not known, we have made no attempt to identify any of the satellite lines.

e. Relative intensities of He-like resonance lines from various elements. The strength of the He-like resonance line increases rapidly with decreasing Z for the plasmas produced in the vacuum spark. For Ti its peak approaches that of $K\alpha$, while for Mo it was not observable. It was not practical to compare the He-like resonance lines from the different elements directly. Instead the peak intensity of the resonance line for a given element was compared with the peak intensity of the plasma $K\beta$ radiation from the same element, and the ratios were plotted vs Z on a semilog scale. If the resulting straight-line relationship continues for higher Z, the He-like resonance line for Mo would be more than 100

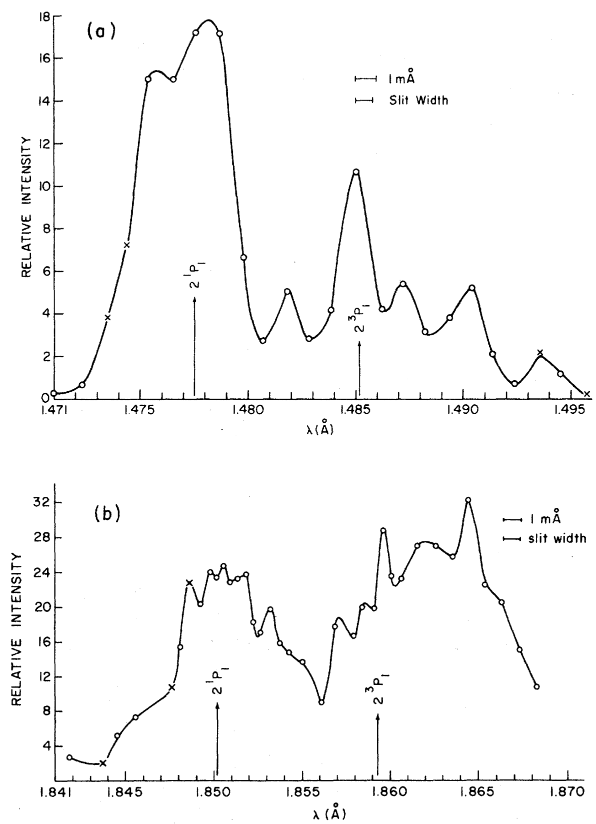

FIG. 4. He-like resonance and Li-like satellite lines [monitor position in brackets]: (a) Cu [1.4770 Å], (b) Fe [1.8510 Å]. Intensity and wavelength errors for the He-like features are as in Fig. 2. Estimated intensity errors for the Li-like features are ~20%. The vertical arrows indicate the predicted positions of resonance lines (upper level $2\,^1P_1$) and intercombination lines (upper levels $2\,^3P_1$) according to Ermolaev (Ref. 11). The forbidden lines (upper levels $2\,^3P_2$, not indicated) would be expected (Ref. 11) between resonance and intercombination lines.

times weaker than the $K\beta$ line of the same element. Since also the $K\beta$ line intensities themselves decrease, although only slowly with increasing Z, the corresponding factor for the absolute He-like line intensity is even larger. (Remember that the term "He-like resonance line" used here may actually refer to a blend of lines as discussed in paragraph *c*.)

C. Electron and ion temperatures

The electron energies found in the vacuum spark bear no direct relationship to the charging voltage, and could in fact be more than ten times the corresponding voltage drop. In any case, the voltage across the gap drops to almost zero as soon as the current is established. The (partial) interruption of the current could, however, give rise to extremely high transient voltages across the gap. This is discussed in more detail in Sec. IV, where it is argued that the x rays are produced when a high-energy electron beam impinges on a cold plasma or metal vapor. Consequently a high-energy nonthermal component is found in the x-ray continuum radiation from the plasma.

We have used the two-foil absorption method with Elton's tables[15] to estimate the electron temperature, assuming a single Maxwell distribution. The following absorber combinations were used: (i) Au: 0.015 and 0.025 in.; (ii) Al: 1 and 3 in.; (iii) Ni: 0.1 and 0.25 in. When the gold absorbers were used with Mo, Cu, and Fe electrodes, no significant difference between these elements in the apparent temperature distributions from shot to shot was found. The median apparent electron temperature was about 40 keV. A two-mode nature of the vacuum spark mechanism is suggested by the distribution of the number of shots within a certain amplitude interval as function of this amplitude, e.g., for the 0.015-in. gold absorber, and perhaps also by the temperature distributions obtained. Using the nickel absorbers, the median temperature is about 15 keV. Aluminum absorbers give a median temperature of about 25 keV. The temperature characteristic of the bulk of the electrons in the x-ray-producing plasma is therefore probably less than 15 keV. Although one cannot rule out the possibility of these various temperatures to be characteristic of different spatial and time domains, these results are also suggestive of two- or multi-component electron velocity distributions.

As indicated in Sec. III B c the narrowest lines measured had *true* half-widths of about 1.4 mÅ or less. If this is taken to be due to Doppler broadening, one gets an ion temperature of almost 10 keV. [$\Delta\lambda/\lambda = 7.7\times10^{-5}(T/\mu)^{1/2}$ with $\mu \simeq 60$ and T in eV]. This is probably an upper limit for the ion temperature in view of the possibilities of blends and other line-broadening mechanisms. Note that some apparent broadening could also be caused by lateral motion of the plasma (see Sec. II). Self-absorption, on the other hand, seems unlikely even for the strongest lines.

D. Electron density measurement

Owing to the small size, short lifetime, and high density of the hot plasma region in the vacuum spark, the usual ways of measuring the electron density are not applicable. Various workers[1-6] have estimated the density somewhere between 10^{19} cm^{-3} and a few times 10^{21} cm^{-3}. In Sec. IV it will be argued that the high-density plasma region is most likely heated by an intense electron beam. Under such conditions, longitudinal waves with frequencies somewhat larger than the Langmuir plasma frequency ω_p will be generated in the plasma. It is well known[16,17] that in a plasma with strong longitudinal waves present, these waves can be coupled to transverse waves near $2\omega_p$. The enhancement of the normal bremsstrahlung near this frequency can be considerable. By scanning the radiation from the plasma over the appropriate wavelength region, one can determine the electron plasma frequency and hence the electron density.

The feature that one should then look for is a sharp increase in radiation at a certain wavelength and coincident in time with the x-ray burst. The wavelength region from 5000 to 9000 Å, which covers either ω_p or $2\omega_p$ corresponding to densities from 4×10^{21} cm^{-3} down to about 2×10^{20} cm^{-3}, was first scanned.

For this purpose, a $\frac{1}{4}$-m monochromator in conjunction with a photomultiplier with S-1 response was used. A preliminary scan, with the monochromator aimed at right angles to the discharge axis, showed that in the wavelength region 7000–8000 Å, many discharges showed features that could be interpreted as enhancement correlated with x-ray-producing pinches.

By means of a beam splitter and a second monochromator, the light output near 5500 Å was observed as a monitor. (The radiation between 3500 and 6000 Å did not show any signs of enhancement.) In Fig. 5 the bottom trace shows a typical scanner signal at 7600 Å, while the top trace shows the monitor signal. The sudden onset of the signals at about 500 nsec from the beginning of the sweep is coincident with the x-ray burst from the discharge. Scanner signals of the type shown in Fig. 5 were most often observed in the wavelength range 7200–8000 Å. The data were analyzed in the following way. The monitor signal was multiplied by the appropriate factor in order to match it to the scanner signal at about 2 μsec after the sudden onset of the radiation, by which time the scanner signal could be assumed to be free from any enhancement. (The enhancements last typically ~200 nsec suggesting that electron density and turbulence decay more slowly than the electron temperature.) This normalized monitor signal was then subtracted from the scanner signal at the peak. The spectrum was scanned in steps of the slit width (250-Å), and six shots were taken at each wavelength position. The difference between the scanner and (normalized) monitor signals was measured (at scanner signal peak) for each shot and the average taken. These values were multiplied by the filter-photomultiplier-monochromator calibration factor (which happened to be nearly constant over the wavelength region concerned). The average enhancement over the background radiation was thus obtained, and the results are plotted in Fig. 6. The peak enhancement over the background was about 80% of the background signal. The half-width of the "line" in Fig. 6 is about 1000 Å. On the wings of the plasma "line" only a small fraction of the discharges gave rise to enhancement (a large difference between the two signals). Consequently, the percentage standard deviation on the values given in Fig. 6 is much larger on the wings (e.g., about 80% at 7200 Å) than near the peak of the line (about 30% at 7600 Å). These standard deviations do not reflect measurement errors but rather real individual characteristics of the various discharges.

Since the results described above supply evidence for actual enhancements of the continuum radiation near 7600 Å, and since we have established that there was no enhancement near or below 4000 Å, we investigated the region 1–1.5 μm to look for enhancement at wavelengths corresponding to ω_p. (This could be caused by scattering of Langmuir waves on lower-frequency waves or disturbances.) Although an increase in the continuum beyond ~1 μm had been seen earlier,[4] no clear evidence for such enhancement could be found, perhaps because ion plasma waves, etc., are relatively weak. There is also a possibility that radiation near the plasma frequency is strongly absorbed under conditions prevailing in the vacuum spark. While classical inverse bremsstrahlung would suggest only ~10% absorption somewhat (~10%) above ω_p, strong Langmuir turbulence may well increase this value by a substantial factor.

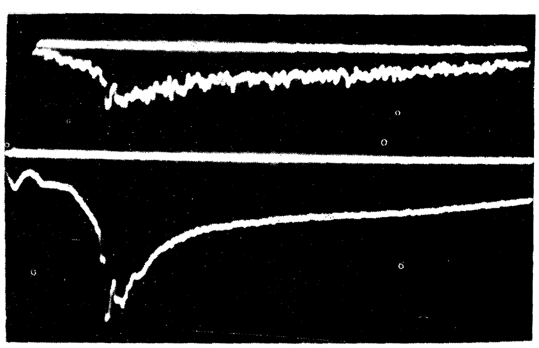

FIG. 5. Enhanced bremsstrahlung from the vacuum spark. Top trace: monitor signal at 5500 Å. Bottom trace: radiation at 7600 Å. Total sweep length: 4.5 μsec.

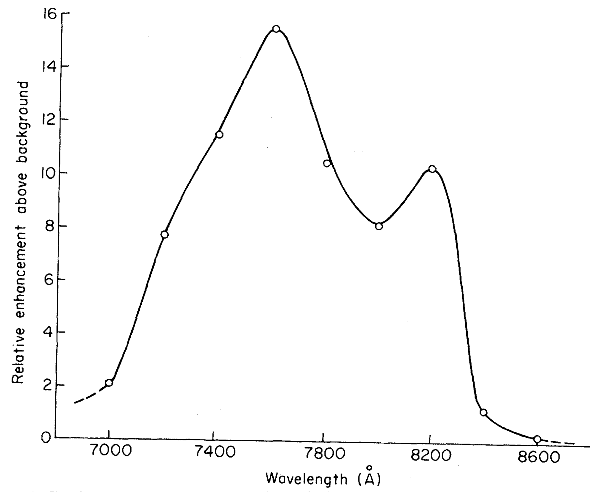

FIG. 6. Average normalized difference between monitor signals and scanner peak intensities vs wavelength.

In the light of the above, we interpret the intensity increases at 7000–8000 Å as corresponding to collective bremsstrahlung at $2\omega_p$. If the wavelength of 7600 Å is taken as representative, the corresponding electron density is calculated as $\sim 5\times10^{20}$ cm^{-3}. (Note also that the observed relative band width of ~15% may correspond to having strong Langmuir wave excitation between ω_p and $\sim 1.3\omega_p$.)

It might perhaps be questioned whether the radiation observed is not due to harmonics in the cyclotron radiation, whose fundamental would correspond to $\lambda \approx 10$ μm at, e.g., 10 MG. Magnetic fields of this order would be consistent with a magnetohydrodynamic Z-pinch model (see Sec. IV), but then the observed radiation would correspond to such a high harmonic that the absence of neighboring harmonics would be inexplicable. Independent evidence for our interpretation and the resulting estimate of the electron density are discussed next.

In Figs. 4(a) and (b), it can be seen that the He-like intercombination line ($2\,^3P_1$-$1\,^1S_0$) is present while, in contrast to coronal spectra, the forbidden line ($2\,^3P_2$-$1\,^1S_0$) is weak or absent. The $2\,^3P_2$ level is depopulated radiatively to $1\,^1S_0$, or collisionally (mainly) to $2\,^3S_1$. After further collisional excitation-energy transfer from $2\,^3S_1$ to $2\,^3P_1$, there follows the rapid radiative decay to $1\,^1S_0$. If there are enough collisions, the population of $2\,^3P_2$ will leak away to $1\,^1S_0$ via $2\,^3S_1$ and the intercombination line, rather than via the forbidden line. A criterion mainly in terms of N_e, making these two decay paths equally likely, leads to a minimum value of N_e. Taking T as 10 keV, this gives a minimum value for N_e of $\sim 3\times10^{20}$ cm^{-3}. (For Fe, rather than Cu, the critical density is[14] slightly below 10^{20} cm^{-3}.) The value of $N_e = 5 \times 10^{20}$ cm^{-3} obtained from the enhanced bremsstrahlung method satisfies this condition. (The actual condition is $\frac{1}{3}\langle\sigma v\rangle N_e = A$, where σ is the inelastic $2P \rightarrow 2S$ cross section,[18] v the electron velocity, and A the radiative decay rate of $2\,^3P_2$, $\sim 1.5\times 10^{10}$ sec^{-1} for $Z = 29$. The $\frac{1}{3}$ factor represents the branching ratio for the $2\,^3S_1 \rightarrow 2\,^3P_1$ collisional transition as a fraction of all $2\,^3S_1 \rightarrow 2\,^3P_J$ transitions. Note also that under "low" density conditions the forbidden line is stronger than the intercombination line.)

E. "Fast time-resolved" measurements of the x-ray emission from the vacuum spark

Measurements by other workers[5,6] indicate that the x rays are not emitted in one pulse, but rather in short bursts lasting only a few nanoseconds. We were interested in finding out the relative times of appearance and lifetimes of the various x-ray emissions. The 1P28 photomultiplier tubes in each of the two monochromators had rise times of 2 nsec.

Two fast oscilloscopes with plug-ins giving a rise time of 0.8 nsec allowed us to observe rise times as short as 3 nsec. The two scopes were triggered by a common source (hard x rays from the vacuum spark), and the relative lengths of the cables from the two monochromators were adjusted to give signals that started within a given small interval of each other on the two scopes when both monochromators were on the $K\alpha$ line. The magnitude of this interval was determined by taking about 20 shots with the monochromators both on $K\alpha$. One monochromator was then kept on $K\alpha$, and the other one put on the line of interest. In this way the relative starting times of the He-like resonance line and Li-like satellites relative to that of $K\alpha$ radiation from the plasma were studied. It was also of interest to find the relative time of onset of the hard x rays.

An external (to the vacuum) photomultiplier-scintillator with only a thin (5-mil Al) window was used to monitor the x rays from the spark. Under these conditions, the most important contribution (and also the earliest in time) was the $K\alpha$ radiation. (This was confirmed by comparing the time history of this signal with that of the $K\alpha$ radiation from the monochromator.) The external photomultiplier signal was synchronized with the $K\alpha$ monitor as before. Gold foils, adding one at a time, were placed in front of the external photomultiplier, and about five shots were taken for each thickness.

The main points of interest about the results of these measurements were the following. The He-like resonance line started about 3 nsec later than $K\alpha$, reached a peak at about the same time as $K\alpha$, but decayed more rapidly than $K\alpha$, as shown in Fig. 7(a). No significant difference between the He-like resonance line and Li-like satellite lines could be detected. The hard x rays behaved differently from the He-like resonance line in that the pulse became narrower with increasing number of absorber foils, but the starting time relative to $K\alpha$ remained the same. In Fig. 7(b), superimposed traces of $K\alpha$ and hard x rays are given. [The traces in Figs. 7(a) and (b) were obtained from single shots.]

The smallest half-width observed for the hard x rays was about 3 nsec, which was near the limit of time resolution for the apparatus. The hard x rays could therefore have lasted less than, say, 1 nsec. The above experimental facts may be interpreted as follows. The heating of the plasma (presumably shown by the hard x rays) lasts for 3 nsec or less. The $K\alpha$ radiation starts simul-

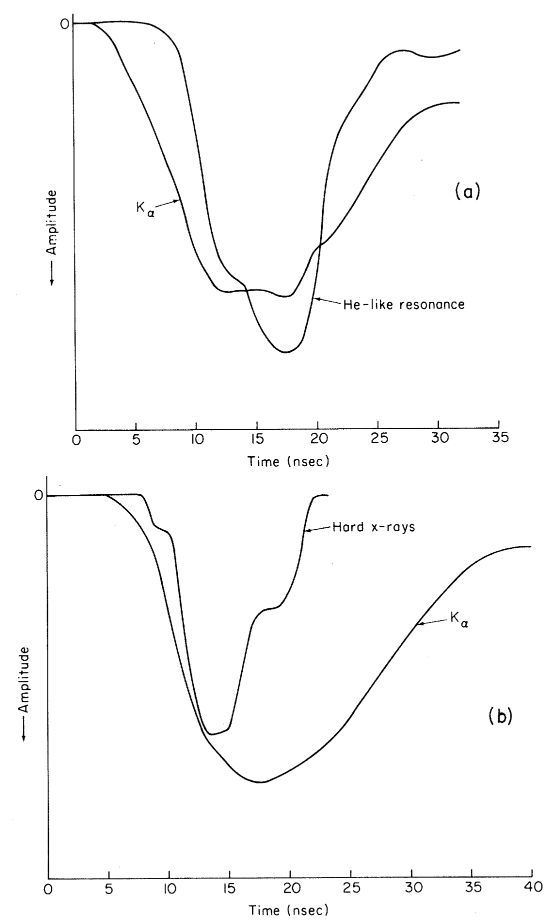

FIG. 7. Fast oscilloscope traces. (a) simultaneous Cu He-like resonance line and Cu $K\alpha$; (b) simultaneous hard x rays (through 0.020-in Au) and Cu $K\alpha$.

taneously with the hard x rays but has a half-width of about 20 nsec. The He-like resonance line does not start until about 3 nsec after the heating pulse. If the electron temperature is assumed to rise instantaneously to about 10 keV, one can estimate how long it should take for the He-like ions to appear. This ionization "delay" time turns out to be only ~0.2 nsec, assuming ionization rate coefficients of Lotz[19] for M- and L-shell electrons, and an initial singly ionized Cu plasma with $N_e=N_i=2\times10^{19}$ cm^{-3}. (All "new" electrons are contributing to the ionization at the same temperature in this model.) More likely than not, the ~3-nsec delay of He-like emission is therefore associated with the macroscopic evolution or spatial structure of the plasma.

IV. MECHANISMS FOR X-RAY PRODUCTION IN THE VACUUM SPARK

The measurement of either the current or its rate of change shows that the x-ray production is always accompanied by a very sudden decrease in current. The rate of change of current at this time could be many times that at the beginning of the discharge.

If the spark is regarded simply as a Z pinch in which the particle pressure is balanced by magnetic pressure, the following conditions might prevail at $N_e=5\times10^{20}$ cm^{-3} and $T_e=10$ keV: radius of pinch $r=40$ μm, magnetic field $B=12$ MG, current density $j=10^{10}$ A cm^{-2}. Such a discharge would, however, suffer from the gross MHD instabilities common to Z pinches. It may be argued that it is just such an instability that gives rise to an abnormally high local electron temperature. There are, however, a number of observations that are best explained by another model discussed below. We note further that inertial containment times of 10-keV Cu ions in a region of ~50 μm are ~0.25 nsec. This is sufficiently long for removal of most M- and L-shell electrons but too short for K-shell ionization, the characteristic time[19] for which is near 3 nsec at our plasma conditions. The failure to detect H-like lines and the duration and strength of He-like emissions therefore suggest that the x-ray-producing plasma has a complex structure, each region or element having a lifetime, say, between 0.1 and 1 nsec. (Weak H-like Fe lines have been observed photographically.[3,6] They would then be associated with an occasional longer-lived region. Note also that in corona equilibrium, predicted[20,21] abundances of He- and H-like Cu ions are comparable at $T_e\approx12\pm2$ keV.)

In Fig. 8, a typical signal from a Rogowski pickup loop (dI/dt) is given on the bottom trace, while the top trace shows simultaneous Cu $K\alpha$ radiation. The rate of change (decrease) of current correlated with strong $K\alpha$ emission could be more than five times that after the breakdown phase, when it is about 5×10^{11} A sec^{-1} and corresponds to the charging voltage of 10 kV. (It is possible that, owing to limitation of the frequency response of the Rogowski coil, the rate of sudden change of current is even higher than indicated by the oscilloscope traces.) Integrating the Rogowski coil signal shows that the current does not go to zero, but drops by about one-third in less than 10 nsec.

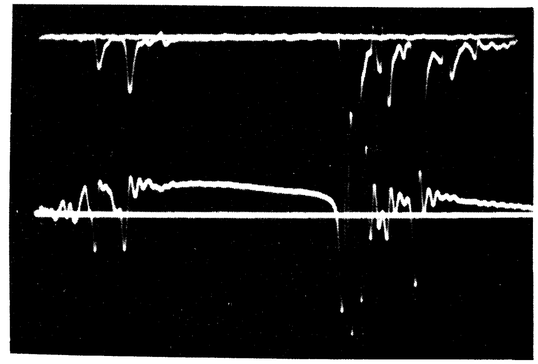

FIG. 8. Oscilloscope traces of Cu $K\alpha$ radiation (top trace) and dI/dt signal from Rogowski loop (bottom trace). Total sweep length is 2 μsec.

As far as production of x rays is concerned, the following was noted. Anode K radiation was produced during the breakdown phase for charging voltages as low as one-third of that corresponding to the energy required to generate the radiation. The most intense radiation during this period usually occurs towards the end of that phase (~400 nsec). Hardly any x rays are ever produced during the next 400–500 nsec. At high charging voltages (>8 kV), the most intense x rays and highest ionization stages are observed near or after 1 μsec, but well before the time-averaged current peaks, and x rays are produced only occasionally near the end of the current rise (~2 μsec). At low charging voltages (3–5 kV), distinct K-radiation pulses are produced also at this late time, and the radiation is then often the most intense.

The mechanisms for production of x rays in the vacuum spark seem to be complicated. Our observations suggest that electron beams play an important role in the process. Electron beams, amongst other possible mechanisms, were also mentioned by Lee.[6] We shall now present evidence for the existence of the beams and shall speculate briefly on the mechanism for generating them.

In order to establish the existence of the beams an iron anode, modified as shown in Fig. 1 (insert), was used. The idea was that fast electrons (if they were present) would stream through the 0.8-mm-diameter hole down the axis and generate $K\alpha$ radiation when they hit the 45° inclined target at the bottom of the hole. These x rays would be detected by monochromator A, while monochromator B would detect $K\alpha$ radiation generated anywhere within the gap. If during a particular discharge x rays are detected by A but none by B, one could conclude that the target was hit by fast electrons and also that the beam diameter was less than 1 mm. On the other hand, a signal from B and none from A would indicate, firstly, that any beam would have been stopped somewhere above the anode tip and, secondly, that A did not see any scattered x rays from above the anode tip. [A Cu target was first used and A and B adjusted to Cu $K\alpha$ and Fe $K\alpha$, respectively. In this way the possibility of A seeing scattered (Fe $K\alpha$) radiation could be eliminated. However, only the first few shots gave Cu $K\alpha$, because the target acquired a coating of iron. Scattered x rays turned out to be no problem, as is evidenced by the fact that many shots were observed where B registered extremely intense x rays and A simultaneously vanishingly small intensity. Rotating the electrode through 90° made the signal on A disappear completely.]

In Fig. 9, typical oscilloscope traces showing signals from monochromator A (top trace) and monochromator B (bottom trace) are given. The relative sensitivity of the oscilloscope channels was adjusted to give about the same peak intensity on both traces; thus the sensitivity on the top trace was 2.5 times that on the bottom trace. These traces may be explained in the following way. During the breakdown phase a pulsed electron beam forms and easily penetrates the low-density metal vapor plasma that exists above the anode at that time, producing relatively small x-ray flux above the anode. (A 10-keV electron, e.g., has a stopping distance of about 4 mm in an iron vapor of atomic density 10^{19} cm^{-3}.) At the time of the second x-ray pulse the metal vapor must be much denser than this, and practically all electrons are stopped above the anode, as is indicated by the strong pulse from B and weak pulse from A. During the last (third) pulse from B (Fig. 9), the pulse from A has almost vanished.

From the two-foil absorption measurements (Sec. III C), we infer photon energies as high as 100 keV. This may show that either very high rates of compression of the current channel occur, or that a high-voltage low-impedance energy source is available to drive an intense electron beam for times of the order of 10 nsec or less. While

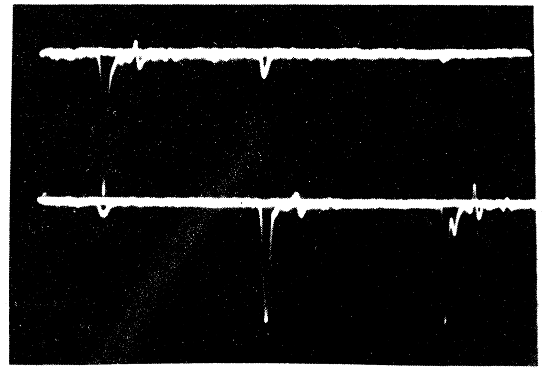

FIG. 9. $K\alpha$ radiation from the modified anode in Fig. 1. Top trace: monochromator A (200 mV/cm). Bottom trace: monochromator B (500 mV/cm). Total sweep length is 2 μsec.

pinching of the current channel may play an important intermediate role in the production of the x rays, as is suggested below, the relatively low ion temperature may argue against it as the basic mechanism. On the other hand, there is the evidence for the existence of intense electron beams within the gap as explained in the previous paragraph. Owing to, e.g., the two-stream instability, electron beams can transfer their energy to the surrounding plasma over very short distances. The question then is how these beams are generated. A very much simplified explanation may be the following. During the breakdown of the gap a cold metal vapor is formed through the bombardment of the anode by electrons. Ions moving towards the cathode (in about 100 nsec at 10 kV) will create a plasma also near the cathode. When this plasma is dense enough to supply the required current, breakdown of the gap is complete. However, the current is still carried mainly by electrons through the "vacuum" between the anode and cathode plasmas. (The light output from the discharge stays relatively weak until the main x-ray burst, as is clear from Fig. 5.) Since the current channel is non-neutral, it will not be compressed substantially. However, where it meets the anode plasma, charge neutralization will occur and the electron current will be focused on to the anode plasma.

This localized pinching continues as long as the external magnetic pressure is unbalanced by the plasma pressure. Due to the decrease of the cross section of the current channel, and hence the increase of the local anomalous *resistance*, the current drops suddenly by about 30%, which in turn gives rise to a very high induced voltage across the gap. For a *total* circuit *inductance* of 20 nH (mostly in series with the gap) and a current change from 150 to 100 kA in 10 nsec, the induced (forward) voltage across the gap is 100 kV. (Owing to the localization of the pinch, the reverse induced voltage resulting from the increase in inductance during the pinch is believed small, although induced electric fields in this region may be substantial.) The magnetic energy available is about 100 J (when the current drops from 150 to 100 kA). The power is therefore of the order of 10^{10} W or more, depending on how rapidly the current changes. Assuming characteristic linear dimensions of 100 μm, the corresponding power per unit area is thus seen to be $\gtrsim 10^{14}$ W/cm^2, comparable with those of high-power lasers. The electron kinetic energy in a sphere of diameter 100 μ, electron density 5×10^{20} cm^{-3}, and temperature 10 keV is only about 5 J. (The ionization energy is negligible, even for complete stripping, e.g., of Cu.) This implies that there is enough energy available from the magnetic field for a number of x-ray bursts. Because of the high anomalous resistance of the plasma, the magnetic energy can be dissipated rapidly. Since the electrons undergo very few collisions with ions or atoms until they encounter the anode plasma, practically all their energy will be deposited within a very small volume. If the metal vapor is of low density, as it is during breakdown, most of the electrons hit the anode itself, causing a small-diameter hole, as seen on all anodes after 20 discharges or so. In this way the vapor density is increased, the vapor cloud expands away from the anode, and the pinching and high-energy beam formation could repeat several times. Only towards the end of this phase does the cloud reach the cathode, and because of high vapor density and hence high collision rates, electron beams no longer form. Thus, this model also explains why, for x-ray production to occur, at least part of the gap between the electrodes must be as good a vacuum as possible. (At low charging voltages, not enough metal vapor is formed from the anode to fill the gap, and x rays are produced until right up to the current peak.)

V. CONCLUSION

The vacuum-spark apparatus that we used was found to be capable of generating plasmas with electron density $\sim 5\times10^{20}$ cm^{-3} and electron temperature $\lesssim 15$ keV. (Ion temperatures were estimated to be $\lesssim 10$ keV.) The combination of temperature, density, and lifetime of the plasmas was such that measurable He-like lines of elements with atomic numbers up to $Z=29$ were generated. For none of the elements studied ($Z\geqslant 22$) could we detect any hydrogenlike lines with significant intensity above the background. The He-like resonance lines seem to be broadened (or enhanced) considerably, most likely through blending with Li-like satellite lines. The main characteristics of the x rays and plasmas produced by the vacuum spark can be explained in terms of the interaction of high-energy pulsed electron beams with a cold vapor or plasma emerging from the anode. Such a model for plasma and x-ray production in low-inductance sparks, although far from complete, is supported by various results reported by other workers, especially by Lee.[6,22]

---

*Supported by Atomic Energy Commission (ERDA) and National Science Foundation.

†Permanent address: Physics Department, University of Cape Town, Cape Town, South Africa.

[1] L. Cohen, U. Feldman, M. Swartz, and J. H. Underwood, J. Opt. Soc. Am. 58, 843 (1968).

[2] T. N. Lie and R. C. Elton, Phys. Rev. A 3, 865 (1971).

[3] J. L. Schwob and B. S. Fraenkel, Space Sci. Rev. 13, 589 (1972).

[4] J. J. Turechek and H.-J. Kunze, Z. Phys. (to be published); see also J. J. Turechek, University of Maryland Technical Report 73-083 (unpublished).

[5] S. K. Handel and J. M. Berg, Ark. Fys. 21, 1 (1966); S. K. Handel, Ark. Fys. 28, 27 (1965).

[6] T. N. Lee, Ann. N. Y. Acad. Sci. 251, 112 (1975).

[7] L. L. House, Astrophys. J. Suppl. Ser. 18, 21 (1969).

[8] E. Clementi, IBM J. Res. Dev. 9, 1 (1965).

[9] B. S. Fraenkel, M. Klapisch, J. L. Schwob, IAU Colloquium No. 27 (1974).

[10] A. M. Ermolaev, M. Jones, and K. J. H. Phillips, Astrophys. Lett. 12, 53 (1972).

[11] A. M. Ermolaev, Phys. Rev. A 8, 1651 (1973).

[12] A. H. Gabriel, Mon. Not. R. Astron. Soc. 160, 99 (1972).

[13] H. P. Summers, Astrophys. J. 179, L45 (1973).

[14] A. H. Gabriel (private communication).

[15] R. C. Elton, Report 6738, Naval Research Laboratory, Washington, D. C., 1968.

[16] C. A. Chin-Fatt and H. R. Griem, Phys. Rev. Lett. 25, 1644 (1970); C. A. Chin-Fatt, Phys. Fluids 17, 1410 (1974).

[17] R. S. Post and T. C. Marshall, Phys. Fluids 17, 452 (1974).

[18] H. R. Griem, *Spectral Line Broadening by Plasmas* (Academic, New York, 1974).

[19] W. Lotz, Astrophys. J. Suppl. Ser. 14, 207 (1967).

[20] D. Mosher, Phys. Rev. A 10, 2330 (1974).

[21] H. P. Summers, Mon. Not. R. Astron. Soc. 169, 663 (1974).

[22] T. N. Lee, Astrophys. J. 190, 467 (1974); see also J. Fukai and E. J. Clothîaux, Phys. Rev. Lett. 34, 863 (1975).

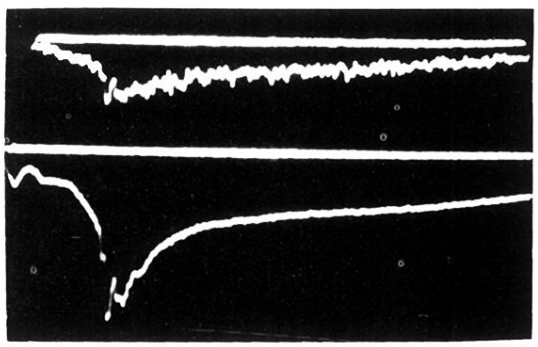

FIG. 5. Enhanced bremsstrahlung from the vacuum spark. Top trace: monitor signal at 5500 Å. Bottom trace: radiation at 7600 Å. Total sweep length: 4.5 μsec.

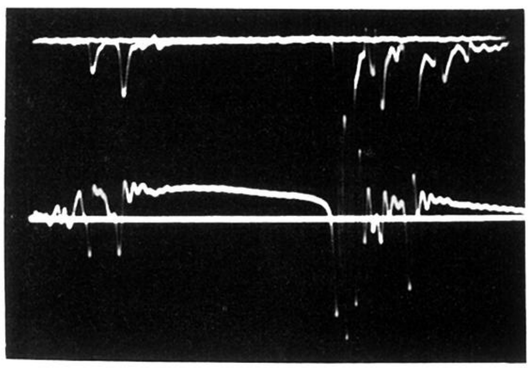

FIG. 8. Oscilloscope traces of Cu $K\alpha$ radiation (top trace) and dI/dt signal from Rogowski loop (bottom trace). Total sweep length is 2 μsec.

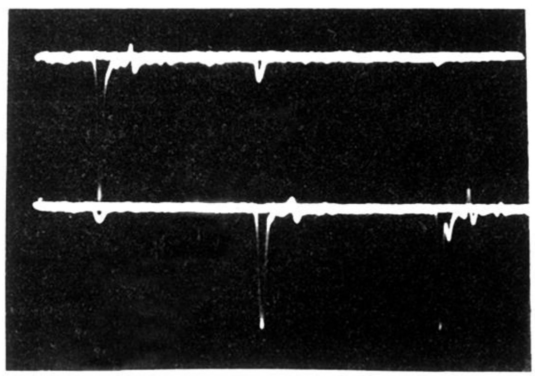

FIG. 9. $K\alpha$ radiation from the modified anode in Fig. 1. Top trace: monochromator A (200 mV/cm). Bottom trace: monochromator B (500 mV/cm). Total sweep length is 2 μsec.